# Remodeling Tumor Vasculature to Enhance Delivery of Intermediate-Sized Nanoparticles

Wen Jiang,[†,⊥] Yuhui Huang,[#,‡,⊥] Yi An,[§] and Betty Y. S. Kim[*,‡]

[†]Department of Radiation Oncology, The University of Texas MD Anderson Cancer Center, Houston, Texas, United States, [#]The Cyrus Tang Hematology Center, Jiangsu Institute of Hematology, the Collaborative Innovation Center of Hematology, Soochow University, China, [§]Department of Radiation Oncology, Yale-New Haven Hospital, New Haven, Connecticut, United States, and [‡]Department of Neurosurgery, Mayo Clinic College of Medicine, Jacksonville, Florida, United States. [⊥]W. Jiang and Y. Huang contributed equally.

ABSTRACT Restoration of dysfunctional tumor vasculature can reestablish the pressure gradient between intravascular and interstitial space that is essential for transporting nanomedicines into solid tumors. Morphologic and functional normalization of tumor vessels improves tissue perfusion to facilitate intratumoral nanoparticle delivery. However, this remodeling process also reduces tumor vessel permeability, which can impair nanoparticle transport. Although nanoparticles sized below 10 nm maximally benefited from tumor vessel normalization therapy for enhanced nanomedicine delivery, the small particle size severely limits its applicability. Here, we show that intermediate-sized nanoparticles (20−40 nm) can also benefit from tumor vasculature remodeling. We demonstrate that a window of opportunity exists for a two-stage transport strategy of different nanoparticle sizes. Overall, tumor vessel remodeling enhances the transvascular delivery of intermediate-size nanoparticles of up to 40 nm. Once within the tumor matrix, however, smaller nanoparticles experience a significantly lesser degree of diffusional hindrance, resulting in a more homogeneous distribution within the tumor interstitium. These findings suggest that antiangiogenic therapy and nanoparticle design can be combined in a multistage fashion, with two sets of size-inclusion criteria, to achieve optimal nanomedicine delivery into solid tumors.
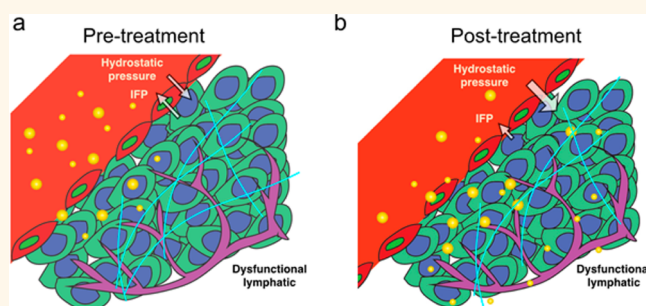
KEYWORDS: antiangiogenic therapy · nanomedicine · tumor delivery · tumor targeting

Successful delivery of nanomedicine into solid tumors is critical to the field of cancer nanotechnology research.[1] Nanomedicine delivery relies on a functional vascular network to enable homogeneous transport of these agents *via* convection- and diffusion-based mechanisms.[2] However, unlike blood vessels within healthy tissues, tumor vessels are often leaky and disorganized; consequently, their ability to deliver drugs, molecules, or cells into the tumor bed is impaired.[3,4] The structural and functional abnormalities of these vascular networks are a direct result of the imbalance between proangiogenic and antiangiogenic signals within the tumor microenvironment, driven by unopposed actions of factors such as vascular endothelial growth factor (VEGF).[5] When properly performed, inhibition of angiogenesis can moderately restore the structural integrity of tumor vessels and facilitate intratumoral delivery of small molecules.[6,7]

Recently, antiangiogenic therapy *via* VEGF receptor-2 (VEGFR-2) blockade was shown to normalize tumor blood vessels and improve nanomedicine delivery.[8] However, on the basis of this study, it was postulated that the "vascular normalization" process was limited to small nanoparticles (∼10 nm) because of increased steric and hydrodynamic hindrance associated with the smaller pore sizes of more mature and normalized tumor vessels.[8] Most synthetic nanoparticles under investigation for biomedical applications exceed this size threshold because of increasing requirements for surface modification to reduce reticuloendothelial system clearance and enhance targeting;[9] thus, this size constraint restricts the clinical utility of tumor vasculature normalization strategies to complement nanomedicine delivery. Here, we hypothesize that the careful restoration of the abnormal tumor vasculatures can also improve the
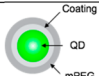
TABLE 1. Nanoparticle Characterization for Intratumoral Delivery

Nanoparticle Type	Structure	Hydrodynamic Diameter (nm)	Surface Charge (eV)	Blood half-life (min)
QD-mPEG2k		19.5±1.2	-2.3±1.1 mV	416
QD-mPEG10K		40.4±3.8	-3.2±1.6 mV	170

delivery and distribution of intermediate-sized nanoparticles into solid tumors. Using fluorescently labeled nanoparticles of size in the 20 to 40 nm range, we aimed to monitor the tumor delivery of these nanoparticles after anti-VEGFR-2 blockade. Further, using multiphoton imaging and fluorescent correlated spectroscopy, we set out to demonstrate that nanoparticles within this size range can also benefit from a vascular normalization process in terms of transvascular transport, but may experience a size-dependent diffusional hindrance once inside the tumor interstitium.

RESULTS

To determine whether the delivery of intermediate-sized nanoparticles with a hydrodynamic diameter of 20 to 40 nm can benefit from a tumor vessel remodeling strategy, we studied the *in vivo* transport dynamics of these nanoparticles using breast tumor models orthotopically implanted in mice and treated with VEGFR-2-blocking antibodies. The selected size range is representative of surface-modified, protein-coated nanoparticles currently used in biomedical imaging applications.[10] Using water-soluble semiconductor nanocrystals (quantum dots, QDs) of similar core size, we adjusted their final hydrodynamic diameter *via* surface modification with polyethylene glycol (PEG) of different molecular weights (Table 1).[11,12] These monodisperse nanoparticles (Supplemental Figure S1) have similar surface charges and a prolonged circulatory half-life (Table 1). When nanoparticles were injected intravenously into syngeneic immunocompetent FVB mice, we noted that the circulation half-life was dependent on the final size after surface coating with PEG, with 20 nm nanoparticles (QD-mPEG2K) showing almost a 2.5-fold increase in circulation half-life compared with 40 nm nanoparticles (QD-mPEG10K) (Table 1; Supplemental Figure S2). As expected, both nanoparticle sizes showed mild to moderate levels of accumulation in the liver, but larger sized QD-mPEG10K had increased hepatic uptake consistent with existing literature (Supplemental Figure S2).[12]

To examine the effect of VEGFR-2 blockade on tumor vasculature, we first orthotopically implanted breast adenocarcinoma MCaP0008 cells into the mammary fat pad of syngeneic immunocompenent FVB mice and imaged tumor vessel changes using intravital multiphoton imaging.[4] After treatment with rat anti-VEGFR-2 antibody (DC101; 10 mg/kg every 3 days), progressive morphologic restoration of tumor vasculature was

observed after 2 days of treatments. Consistent with our previous observations,[4,8] this vascular normalization process was transient, with significant reduction in tumor vessel density by day 8 of treatment (Figure 1A). We quantified the structural changes in tumor vessels after DC101 treatments and showed that it markedly decreased tumor vessel length and volume but maintained vessel diameter (Figure 1B,C). As previously observed, these structural alterations were associated with improved tissue perfusion and increased pericyte coverage, leading to functional vessel restoration (Figure 1D,E; Supplemental Figure S3).[4]

To determine whether restoration of tumor vessel structure functionally improves delivery of intermediate-sized nanoparticles into solid tumors, we intravenously injected QD-mPEG2K and QD-mPEG10K nanoparticles into tumor-bearing mice after 5 days of DC101 treatment. Using intravital imaging, we observed that DC101 treatment improved both QD-mPEG2k and QD-mPEG10k accumulation within the tumor interstitium compared with isomatched immunoglobulin (Ig) G controls (Figure 2). In contrast to previous work that showed nanoparticle accumulation predominantly in the perivascular spaces,[12] DC101 treatment resulted in homogeneous distribution of nanoparticles within the tumor interstitium, irrespective of size. Importantly, although DC101 induced tumor vessel restoration and improved interstitial delivery of QD-mPEG2k and QD-mPEG10k nanoparticles, QD-mPEG2k showed a greater degree of uniform intratumoral accumulation (Figure 2).

To quantify improvement in intratumoral delivery of nanoparticles with tumor vessel normalization, we perfused fluorescein isothiocyanate (FITC)-lectin into DC101-treated mice after injection with QD-mPEG2K and QD-mPEG10K.[4] Laser confocal microscopy showed a greater proportion of functional vessels labeled by FITC-lectin in DC101-treated tumors compared with IgG controls, suggesting improved tumor perfusion after vessel restoration (Supplemental Figure S3). This improved perfusion also enhanced delivery of QD-mPEG2K and QD-mPEG10K into the tumor bed. IgG-treated samples showed perivascular clumping and heterogeneous accumulation of QD-mPEG2k and QD-mPEG10K nanoparticles (Figure 3A). In contrast, DC101 treatment resulted in homogeneous distribution of nanoparticles within the tumor, including areas further from the blood vessels. Improved nanoparticle delivery was due to the increased number of perfusing vessels
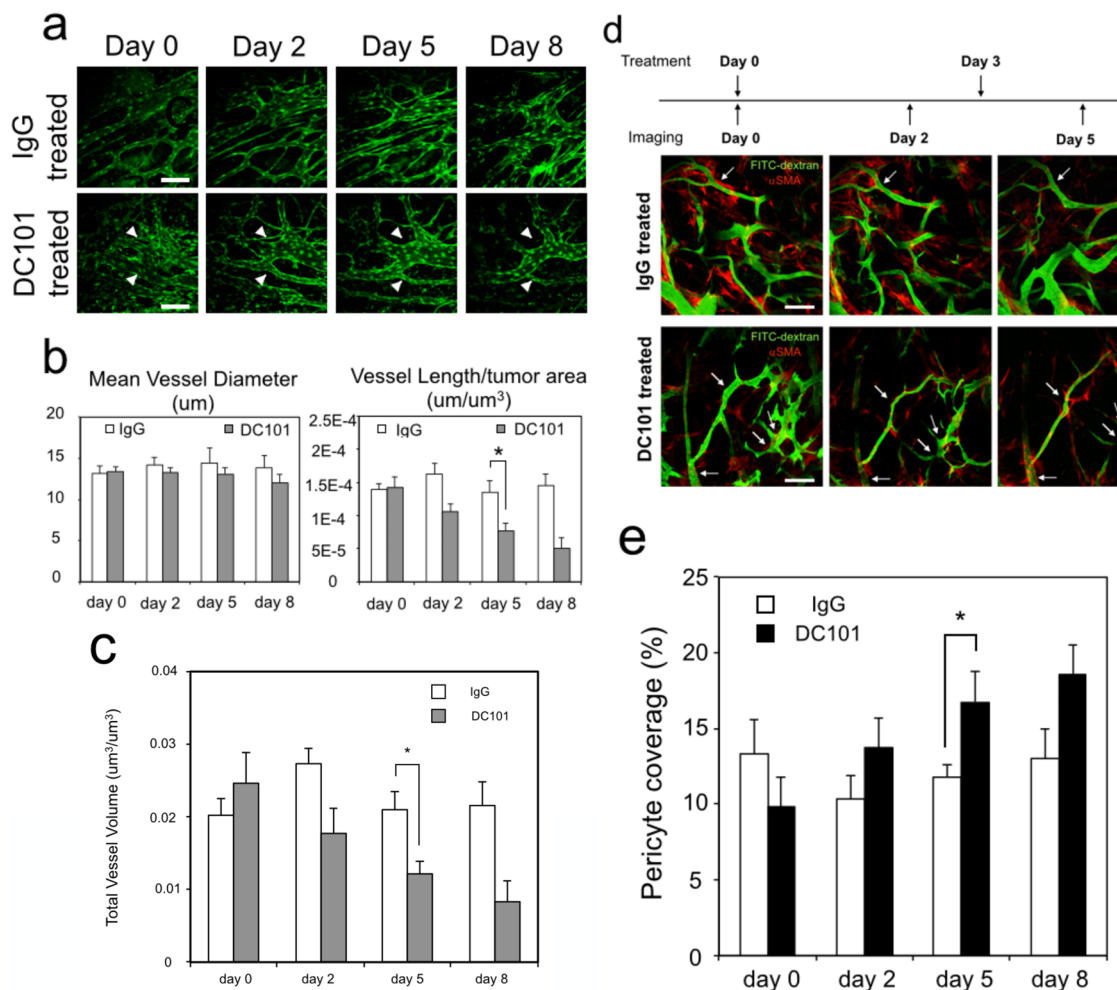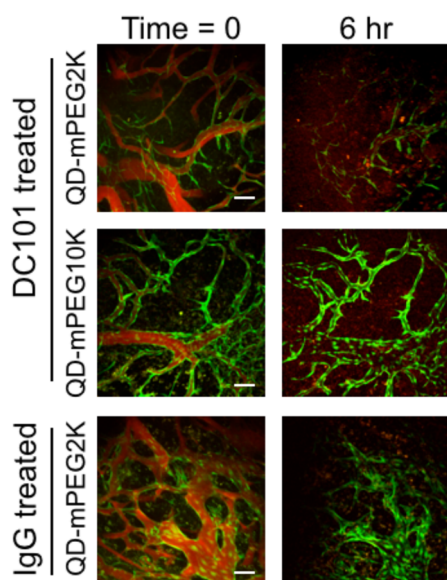
Figure 1. DC101 treatment normalized tumor vasculature and improved pericyte coverage. (A) Serial treatment of MCaP0008 tumor xenograft models with DC101 (antivascular endothelial growth factor receptor-2 antibody) showed progressive normalization of tumor vessel morphology (arrow) compared with immunoglobulin (Ig) G controls. (B) Mean tumor vessel diameter decreased slightly, as did the total vessel length per unit of tumor tissue. (C) Total vessel volume per unit of tumor tissue significantly decreased as a direct effect of the vessel-normalizing effect. (D) DC101 treatment also increased the coverage of pericytes along the endothelial wall (arrow). (E) Increased pericyte coverage with time decreased vascular leakiness and vessel permeability, eventually reestablishing the transvascular pressure gradient. Scale bar = 50 μm; asterisk denotes $p < 0.05$; α-SMA: α-smooth muscle actin; FITC, fluorescein isothiocyanate.

within the tumor bed (Supplemental Figure S3) and to the improved capacity of individual vessels for delivering nanoparticles into the tumor interstitium.

Importantly, conventional and nanoformulated drugs often have limited access to tumor regions that are poorly vascularized, necrotic, and hypoxic, leading to their decreased therapeutic efficacy.[13] However, previous work has suggested that normalization therapy using an anti-VEGF blockade can affect the vascular pore size along the vessel wall through increased pericyte coverage, thereby restricting the transvascular transport of large nanoparticles into the tumor interstitium.[8] Restoration of the structural integrity and functional capacity of abnormal tumor vessels facilitated delivery of intermediate-size nanoparticles (20–40 nm) to greater regions of the tumor and allowed deeper penetration into the tumor bed (Figure 3B,C).

QD-mPEG2K showed better tissue coverage and penetration than QD-mPEG10K after DC101 treatment. The overall tumor accumulation of the nanoparticles after treatments is shown in Supplemental Figure S4.

Within the tumor interstitium, the eventual distribution of nanoparticles is thought to be limited by diffusional hindrance.[14] To assess whether diffusional limitations contribute significantly to delivery of intermediate-sized nanoparticles to the tumor bed after vascular normalization, we measured the intratumoral diffusion coefficient of QD-mPEG2K and QD-mPEG10K *in vivo* using two-photon fluorescence correlation spectroscopy (Figure 4A).[15] In free solution, QD-mPEG2K and QD-mPEG10k had diffusion coefficients (D_0) of 2.9×10^{-7} and 1.3×10^{-7} cm^2 s^{-1}, respectively, which approximates our estimation of diffusion coefficients calculated with the Stokes–Einstein equation

Figure 2. Normalized tumor vessels after anti-VEGFR-2 antibody DC101 treatment. Intravital imaging showed improved tumor tissue perfusion and enhanced intratumoral delivery of QD-mPEG2K and QD-mPEG10K compared with IgG-treated controls. Red signal is from nanoparticles. Scale bar = 50 μm.
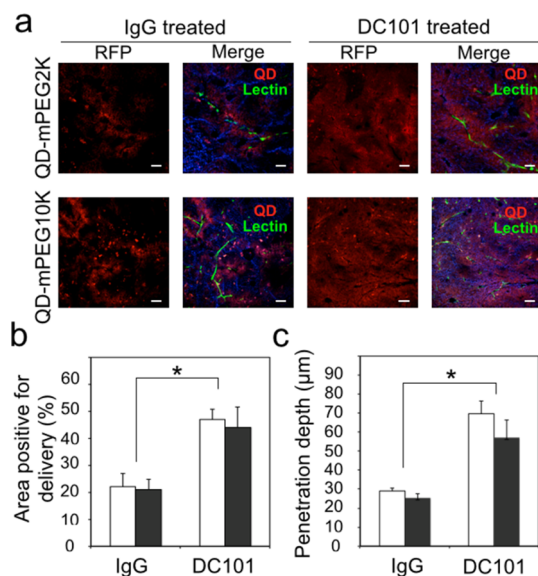
Figure 3. Quantification of improved nanoparticle delivery into tumors after vascular remodeling. (A) DC101 treatment normalized tumor vessels and improved intratumoral delivery and distribution of QD-mPEG2K and QD-mPEG10k nanoparticles. Red channel corresponds to fluorescence of QD-mPEGs, while green signal corresponds to lectin labeling. Quantifying these effects showed that DC101 treatment resulted in increased total tumor area coverage by nanoparticles (B) and increased the penetration depth of nanoparticles into tumors (C). (White bar = QD-mPEG2k, dark bar = QD-mPEG10k.) Scale bar = 50 μm; * denotes $p < 0.05$; Ig, immunoglobulin; RFP, red fluorescent protein.

(for nanoparticles of 20 and 40 nm, diffusion coefficients were 2.5 × 10^{-7} and 1.6 × 10^{-7} cm^2 s^{-1}, respectively) (Supplemental Figure S5). The 2-fold larger coefficient of QD-mPEG2K was due to its being half the
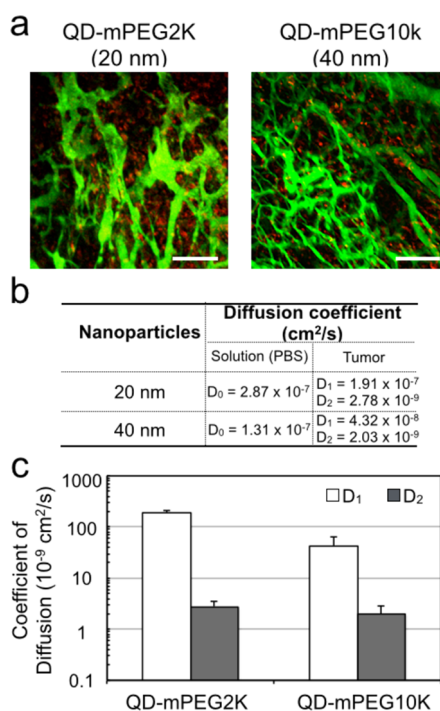
Figure 4. Intratumoral distribution of nanoparticles is size dependent. (A) Although both QD-mPEG2K and QD-mPEG10K had improved delivery into the tumor interstitium after restoration of tumor vessel function, QD-mPEG2K was distributed more homogeneously within the tumor bed. (B, C) Fluorescence correlation spectroscopy was used to determine diffusion coefficients in free solution and within the tumor for QD-mPEG2K and QD-mPEG10K. Here, D_0 is measurement of nanoparticle diffusion in free solution, and D_1 and D_2 are the diffusion coefficients of the fast and slow phases in tumors, respectively. Scale bar = 50 μm; PBS, phosphate-buffered saline.

size of QD-mPEG10K in free solution. In tumors, however, the autocorrelation functions for both types of nanoparticles were best fitted with the two-component diffusion model (Figure 4B; Supplemental Figure S6).[15] This suggests that for both nanoparticle sizes there exist fast (D_1) and slow (D_2) diffusion coefficients corresponding to distinctive sample populations within the viscous and aqueous components of the tumor interstitial matrix.[15,16] The coefficient of diffusion D_1 for QD-mPEG10K was 5 times smaller than that of QD-mPEG2K, but D_2 values were approximately the same. This suggests that within the fluid-like phase of the tumor larger nanoparticles had diffusional hindrance beyond that expected for the increased size (Supplemental Figure S5), whereas in the slow diffusion or gel phase of the tumor tissue, both small and large nanoparticles were restricted to a similar degree.

Analogous observations have been made with other fluorescent tracers composed of bovine serum albumin, 70 kDa dextran, IgG, 2 MDa dextran, and electroneutral liposomes, and the slow diffusion component was attributed to increased collagen and hyaluronan content within the tumor matrix.[15] Here, we showed that these diffusional hindrances are also important obstacles for nanoparticle intratumoral delivery.

The mean D_1/D_0 was noted to be 0.65 for QD-mPEG2k and 0.33 for QD-mPEG10K, whereas D_2/D_0 for both nanoparticles were approximately 2 orders of magnitude slower. This suggests that larger nanoparticles experience increased hindrance within the tumor matrix in addition to the expected decrease in diffusion with increased particle size (Supplemental Figure S5). The use of longer-chain PEGs as a surface coating of QD-mPEG10K compared with QD-mPEG2K may have augmented diffusional hindrance, as previously reported,[15] because shape and conformity can also affect macromolecule diffusion within the tumor matrix. Within the heterogeneous tumor interstitium, the restriction on nanoparticle motion appeared to be predominately observed in the fast diffusion phase, whereas within the slow and viscous phase of the tumor matrix, both QD-mPEG2k and QD-mPEG10K nanoparticles were equally affected (Figure 4B,C).

DISCUSSION

The enhanced and uniform delivery of nanomedicines into solid tumors remains a major challenge in the field of cancer nanotechnology.[17] Nanomaterial-based drug delivery platforms offer many advantages when designing tumor-targeting agents, including robust and easily modifiable surface chemistry and physical properties.[18] However, successful implementation of nanomedicine-based strategies is intricately linked to the functional status of the tumor vasculature. Compared with blood vessels of normal tissues, the vasculature of tumors is leaky, torturous, and disorganized, and as a result, perfusion capacity is impaired.[19] The increased leakiness of tumor vessels is a direct consequence of poor pericyte coverage and enlarged interendothelial junctional distance (range, 40 nm to 1 mm, depending on tumor type).[19] Physiologically, the leaky vasculature is unable to maintain the oncotic and hydrostatic pressure gradients that are normally present between the intravascular and extravascular space.[20] Coupled with the already elevated interstitial fluid pressure within the tumor, the dysfunctional lymphatic system and interstitial fibrosis (among other factors) greatly reduce transvascular flow and limit convection-based transport of macromolecules across the blood vessel walls.[21,22]

Strategies to overcome this barrier to nanoparticle delivery have been investigated, with mixed results.[23-26] Using anti-VEGF receptor 2 antibodies, it was shown that vasculature normalization can improve nanoparticle delivery into solid tumors.[8] Recently, transforming growth factor (TGF)-β inhibitor was also shown to decrease pericyte coverage and increase tumor vessel permeability, which in turn improved nanoparticle delivery.[27] However, both studies have their limitations. In the former, it was concluded that this vascular normalization benefit can only apply to nanoparticles with a diameter of 10 nm or less, as no improvement in

tumor delivery was observed for nanoparticles of 60 or 100 nm.[8] By only examining nanoparticles of these distinctive sizes, the key nanoparticle size range of 20–50 nm, which offers a unique balance between drug payload, targeting, and tissue distribution, was largely ignored. Similarly, in the latter study, the normalization effect was highly dependent on the vascularization status of the tumor, with poorly vascularized pancreatic adenocarcinomas appearing to benefit most from TGF-β inhibition.[27]

Here, we investigated whether an anti-VEGF blockade in breast adenocarcinoma could enhance penetration of intermediate-sized nanoparticles into the tumor and promote uniform distribution in the tumor stroma. We showed that a carefully calibrated dosing schedule of anti-VEGFR-2 antibody facilitated normalization of tumor vessel structure, increased pericyte coverage, and restored perfusion within the tumor interstitium. These physiologic changes in the tumor vasculature increased delivery and penetration of both 20 and 40 nm nanoparticles within the tumor stroma. However, after these nanoparticles reach beyond the blood vessels, smaller sized nanoparticles experience fewer diffusional restrictions from the tumor matrix and ultimately gain greater access to tumor tissues.

As such, these findings present an interesting scenario when designing nanoparticles for intratumoral delivery; specifically, two size-inclusion criteria are needed for transvascular and interstitial transport. First, application of tumor vasculature remodeling strategies improves tumor tissue penetration and delivery for nanoparticles in the 20 to 40 nm size range. Second, once in the tumor interstitium, homogeneous distribution of nanoparticles and their encapsulated cargo requires a smaller size design because of increased restrictions on particle diffusion from the tumor matrix (Figure 5). The development of size-shifting nanoparticles, which decrease in size *via* enzymatic degradation inside the tumor microenvironment, has been reported.[17] This strategy would allow maximal loading of cargo into larger-sized nanoparticles that cross the vascular lumen to the tumor interstitium and then shrink through partial degradation by tumor-secreted proteinases to achieve more homogeneous tissue delivery.[28] Additionally, combination treatments with tumor matrix altering strategies can also promote uniform assess of nanoparticles to the tumor microenvironment. Overall, the advantages of larger nanoparticles (with benefits such as increased functionality, more sophisticated targeting chemistry, and enhanced drug payload) must be balanced against those of smaller nanoparticles (improved pharmacokinetics,[29] tumor delivery,[30] and clearance profiles[31]).

Finally, as demonstrated by others,[27] different tumor types will have distinctive responses to angiogenic therapy, given the specific expression profiles of angiogenic and stromal factors. Therefore, an optimized
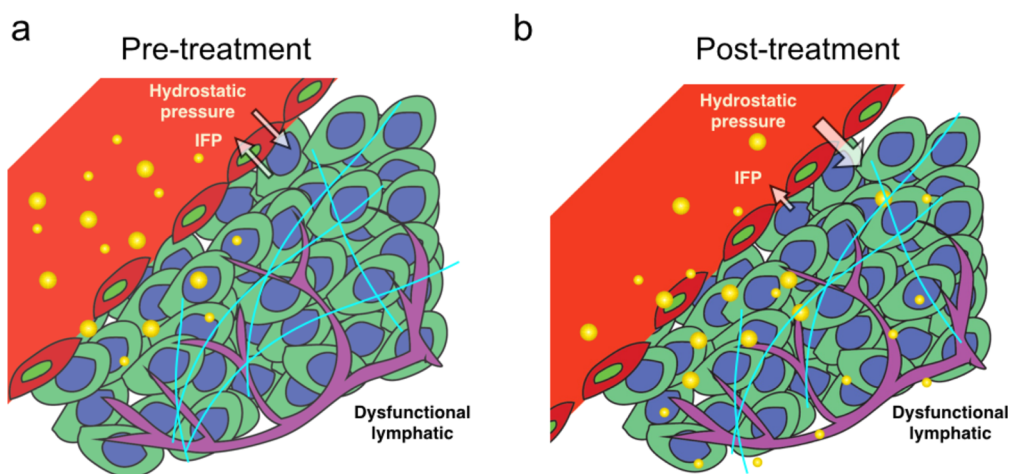
Figure 5. Proposed mechanism of improved nanoparticle delivery into tumors after vessel remodeling. (A) Before treatment, tumor vessels are leaky. With other pathophysiologic features such as impaired lymphatic drainage and increased interstitial fibrosis, the gradient between intravascular pressure and IFP is reduced, leaving nanoparticles (represented as gold circles) unable to penetrate deeper into tumors. (B) Restoration of the structural integrity and function of tumor vessels reestablishes this pressure gradient and improves tissue perfusion, facilitating effective delivery of nanoparticles from the vessel lumen to the tumor interstitium. Once inside the tumor, smaller nanoparticles have less diffusional hindrance from the tumor matrix (light blue lines: collagen) and achieve more uniform distribution and reach deeper areas of the tumor bed. IFP indicates interstitial fluid pressure.

tumor vessel remodeling strategy to enhance nano-medicine delivery must be tailored to the tumor type and perhaps also to the different stages of development for a given tumor. For example, angiogenic switch activation was reported to occur during early stages of colorectal cancer development, between Tis and T1 stages, when local invasion occurs.[32] In contrast, squamous cell carcinoma of the glottic and supraglottic larynx appears to have a higher level of VEGF expression in T2 disease.[33] The temporal relationship between proangiogenic factor production and antiangiogenic blockade needs to be carefully calibrated to manipulate the tumor vasculature normalization window for enhanced nanomedicine delivery.

CONCLUSION

In summary, our study suggests that the combining tumor vasculature remodeling strategy with nanoparticle size design can improve delivery of nanoparticles into solid tumors. Additional characterization of different physical and chemical parameters of delivery vehicles, including surface charge, the addition of targeting moieties, and shape, would provide more detailed insights into designing the most efficient tumor-targeting nanomedicine. Tumor microenvironment modification strategies could potentially provide new design specifications for sophisticated nanomedicine that would lead to more effective and safe cancer therapies.

METHODS/EXPERIMENTAL

Cell Lines and Animals. The breast adenocarcinoma cell line MCaP0008 was obtained from Dr. Peigen Huang (Massachusetts General Hospital). The FVB and Tie2-GFP/FVB transgenic mice were purchased from The Jackson Laboratory. To generate transplanted tumor models, MCaP0008 cells (1×10^6) were injected orthotopically into female FVB mice. When the tumor reached approximately 8 mm in diameter, it was excised and cut into small viable pieces (approximately 1 mm^3) and transplanted orthotopically into the mammary fat pads of female FVB mice. All animal procedures were conducted according to the protocol approved by the Mayo Clinic Institutional Animal Care and Use Committee.

Mammary Fat Pad Window Preparation. Preparation of the mammary fat pad window for intravital multiphoton microscopy was performed as previously described.[4] Briefly, Tie2-GFP/FVB mice were anesthetized and placed on a heating pad. Surgery was performed under sterile conditions by cutting a 15 mm diameter circle of skin from an opposing surface of the mammary fat pad. The exposed fascial plane consisted of epidermis, mammary fat pad, and vasculature. A small piece of tumor tissue was implanted under the fascial layer and covered with a

8 mm glass coverslip attached to a custom-made 10 mm frame.[34] The frame was sutured to the surrounding skin and sealed with cyanoacrylate tissue adhesive.

Nanoparticle Synthesis and Characterization. Water-soluble 585 nm emission carboxy-terminated quantum dots were purchased from Invitrogen Corp. Monofunctional amine-terminated PEG of 2000 and 10 000 MW were purchased from Sigma-Aldrich. Conjugation was performed *via* carbodiimide-mediated chemistry, as described previously.[11] Briefly, a 1:100 ratio of quantum dots:PEG-amine molar mixture was reacted with a 1000:1 molar ratio of N-dimethylaminopropyl-N'-ethylcarbodiimide:quantum dots for 2 h. The finished product was purified using a Sephadex (G-25) column (Sigma-Aldrich). The hydrodynamic diameter and surface charge of purified QD-mPEG2k and QD-mPEG10k were characterized using the Zetasizer Nano ZS90 (Malvern).

Anti-VEGFR-2 Antibody Treatment. After the transplanted MCaP0008 tumors reached a size of 4 to 5 mm in diameter, they were treated with mouse anti-VEGFR-2 antibody DC101 (Eli Lilly) or control rat IgG (Jackson ImunoResearch Laboratories, Inc.) at a scheduled dose of 20 mg/kg of body weight every 3 days for a total of three doses. Tumor volumes were measured by caliper every 3 days and calculated as described previously.[4]

Intravital Microscopy. Blood vessel imaging was performed on days 0, 2, and 5 during treatment using a multiphoton laser-scanning microscope customized for live-animal imaging. For intravital imaging experiments, tumor-bearing mice were anaesthetized and immobilized onto the microscope stage using a custom platform to minimize motion from breathing and circulation. Mice were kept alive on a heating pad and sedated *via* isofluorane inhaled through a nose cone. All images were acquired using a Prairie Ultima IV (Prairie Technologies) upright *in vivo* two-photon microscope equipped with a 10× or 20× water-immersion objective (NA 0.95). Emission filters of 525 ± 25 and 620 ± 30 nm were used for green and red fluorescent protein channels, respectively. All fluorophores were excited with a MaiTai HP Ti:sapphire two-photon laser (~100 fs pulse width), at an excitation wavelength of 900 nm (500 mW).

Conflict of Interest: The authors declare no competing financial interest.

Supporting Information Available: The Supporting Information is available free of charge on the ACS Publications website at DOI: 10.1021/acsnano.5b02028.

Supplemental methods, hydrodynamic radius characterization of the nanoparticles (Figure S1), blood half-life measurements (Figure S2), tumor vessel perfusion measurement (Figure S3), Stokes−Einstein equation (Figure S4), nanoparticle diffusion (Figure S5), tumor uptake (Figure S6), and tumor perfusion measurements (Figure S7) (PDF)

Note Added after ASAP Publication: This paper published ASAP on July 31, 2015. The Acknowledgment section was modified and the revised version was reposted on August 4, 2015.

REFERENCES AND NOTES

1. Ferrari, M. Cancer Nanotechnology: Opportunities and Challenges. *Nat. Rev. Cancer* **2005**, *5*, 161–171.
2. Jain, R. K.; Stylianopoulos, T. Delivering Nanomedicine to Solid Tumors. *Nat. Rev. Clin. Oncol.* **2010**, *7*, 653–664.
3. Chauhan, V. P.; Stylianopoulos, T.; Boucher, Y.; Jain, R. K. Delivery of Molecular and Nanoscale Medicine to Tumors: Transport Barriers and Strategies. *Annu. Rev. Chem. Biomol. Eng.* **2011**, *2*, 281–298.
4. Huang, Y.; Yuan, J.; Righi, E.; Kamoun, W. S.; Ancukiewicz, M.; Nezivar, J.; Santosuosso, M.; Martin, J. D.; Martin M. R.; Vianello, F.; et al. Vascular Normalizing Doses of Antiangiogenic Treatment Reprogram the Immunosuppressive Tumor Microenvironment and Enhance Immunotherapy. *Proc. Natl. Acad. Sci. U. S. A.* **2012**, *109*, 17561–17566.
5. Huang, Y.; Goel, S.; Duda, D. G.; Fukumura, D.; Jain, R. K. Vascular Normalization as an Emerging Strategy to Enhance Cancer Immunotherapy. *Cancer Res.* **2013**, *73*, 2943–2948.
6. Tong, R. T.; Boucher, Y.; Kozin, S. V.; Winkler, F.; Hicklin, D. J.; Jain, R. K. Vascular Normalization by Vascular Endothelial Growth Factor Receptor 2 Blockade Induces a Pressure Gradient across the Vasculature and Improves Drug Penetration in Tumors. *Cancer Res.* **2004**, *64*, 3731–3736.
7. Huang, Y.; Stylianopoulos, T.; Duda, D. G.; Fukumura, D.; Jain, R. K. Benefits of Vascular Normalization are Dose and Time Dependent. *Cancer Res.* **2013**, *73*, 7144–7146.
8. Chauhan, V. P.; Stylianopoulos, T.; Martin, J. D.; Popovic, Z.; Chen, O.; Kamoun, W. S.; Bawendi, M. G.; Fukumura, D.; Jain, R. K. Normalization of Tumour Blood Vessels Improves the Delivery of Nanomedicines in a Size-Dependent Manner. *Nat. Nanotechnol.* **2012**, *7*, 383–388.
9. Peer, D.; Karp, J. M.; Hong, S.; Farokhzad, O. C.; Margalit, R.; Langer, R. Nanocarriers as an Emerging Platform for Cancer Therapy. *Nat. Nanotechnol.* **2007**, *2*, 751–760.
10. Zrazhevskiy, P.; Sena, M.; Gao, X. Designing Multifunctional Quantum Dots for Bioimaging, Detection, and Drug Delivery. *Chem. Soc. Rev.* **2010**, *39*, 4326–4354.
11. Jiang, W.; Mardyani, S.; Fischer, H.; Chan, W. C. W. Design and Characterization of Lysine Cross-linked Mercapto-acid Biocompatible Quantum Dots. *Chem. Mater.* **2006**, *18*, 872–878.
12. Perrault, S. D.; Walkey, C.; Jennings, T.; Fischer, H. C.; Chan, W. C. Mediating Tumor Targeting Efficiency of Nanoparticles Through Design. *Nano Lett.* **2009**, *9*, 1909–1915.
13. Jain, R. K. Normalization of Tumor Vasculature: An Emerging Concept in Antiangiogenic Therapy. *Science* **2005**, *307*, 58–62.
14. Netti, P. A.; Berk, D. A.; Swartz, M. A.; Grodzinsky, A. J.; Jain, R. K. Role of Extracellular Matrix Assembly in Interstitial Transport in Solid Tumors. *Cancer Res.* **2000**, *60*, 2497–2503.
15. Alexandrakis, G.; Brown, E. B.; Tong, R. T.; McKee, T. D.; Campbell, R. B.; Boucher, Y.; Jain, R. K. Two-Photon Fluorescence Correlation Microscopy Reveals the Two-Phase Nature of Transport in Tumors. *Nat. Med.* **2004**, *10*, 203–207.
16. Jain, R. K. Transport of Molecules in the Tumor Interstitium: A Review. *Cancer Res.* **1987**, *47*, 3039–3051.
17. Chow, E. K.; Ho, D. Cancer Nanomedicine: From Drug Delivery to Imaging. *Sci. Transl. Med.* **2013**, *5*, 216rv4.
18. Jiang, W.; Kim, B. Y.; Rutka, J. T.; Chan, W. C. Advances and Challenges of Nanotechnology-Based Drug Delivery Systems. *Expert Opin. Drug Delivery* **2007**, *4*, 621–633.
19. Jain, R. K. Transport of Molecules Across Tumor Vasculature. *Cancer Metastasis Rev.* **1987**, *6*, 559–593.
20. Jain, R. K. Delivery of Molecular and Cellular Medicine to Solid Tumors. *Adv. Drug Delivery Rev.* **2001**, *46*, 149–168.
21. Padera, T. P.; Kadambi, A.; di Tomaso, E.; Carreira, C. M.; Brown, E. B.; Boucher, Y.; Choi, N. C.; Mathisen, D.; Wain, J.; Mark, E. J.; et al. Lymphatic Metastasis in the Absence of Functional Intratumor Lymphatics. *Science* **2002**, *296*, 1883–1886.
22. Heldin, C. H.; Rubin, K.; Pietras, K.; Ostman, A. High Interstitial Fluid Pressure: an Obstacle in Cancer Therapy. *Nat. Rev. Cancer* **2004**, *4*, 806–813.
23. Pietras, K.; Rubin, K.; Sjoblom, T.; Buchdunger, E.; Sjoquist, M.; Heldin, C. H.; Ostman, A. Inhibition of PDGF Receptor Signaling in Tumor Stroma Enhances Antitumor Effect of Chemotherapy. *Cancer Res.* **2002**, *62*, 5476–5484.
24. Lammerts, E.; Roswall, P.; Sundberg, C.; Gotwals, P. J.; Koteliansky, V. E.; Reed, R. K.; Heldin, N. E.; Rubin, K. Interference with TGF-beta1 and -beta3 in Tumor Stroma Lowers Tumor Interstitial Fluid Pressure Independently of Growth in Experimental Carcinoma. *Int. J. Cancer* **2002**, *102*, 453–462.
25. Eikenes, L.; Bruland, O. S.; Brekken, C.; Davies, C. L. Collagenase Increases the Transcapillary Pressure Gradient and Improves the Uptake and Distribution of Monoclonal Antibodies In Human Osteosarcoma Xenografts. *Cancer Res.* **2004**, *64*, 4768–4773.
26. Salnikov, A. V.; Iversen, V. V.; Koisti, M.; Sundberg, C.; Johansson, L.; Stuhr, L. B.; Sloquist, M.; Ahlstrom, H.; Reed, R. K.; Rubin, K. Lowering of Tumor Interstitial Fluid Pressure Specifically Augments Efficacy of Chemotherapy. *FASEB J.* **2003**, *17*, 1756–1758.
27. Cabral, H.; Matsumoto, Y.; Mizuno, K.; Chen, Q.; Murakami, M.; Kimura, M.; Terada, Y.; Kano, M. R.; Miyazono, K.; Uesaka, M.; et al. Accumulation of sub-100 nm Polymeric Micelles in Poorly Permeable Tumours Depends on Size. *Nat. Nanotechnol.* **2011**, *6*, 815–823.
28. Wong, C.; Stylianopoulos, T.; Cui, J.; Martin, J.; Chauhan, V. P.; Jiang, W.; Popovic, Z.; Jain, R. K.; Bawendi, M. G.; Fukumura, D. Multistage Nanoparticle Delivery System for

Deep Penetration into Tumor Tissue. *Proc. Natl. Acad. Sci. U. S. A.* **2011**, *108*, 2426–2431.

29. Albanese, A.; Tang, P. S.; Chan, W. C. The Effect of Nanoparticle Size, Shape, and Surface Chemistry on Biological Systems. *Annu. Rev. Biomed. Eng.* **2012**, *14*, 1–16.

30. Dreaden, E. C.; Austin, L. A.; Mackey, M. A.; El-Sayed, M. A. Gold Nanoparticles in Targeted Cancer Drug Delivery. *Ther. Delivery* **2012**, *3*, 457–478.

31. Choi, H. S.; Liu, W.; Misra, P.; Tanaka, E.; Zimmer, J. P.; Itty Ipe, B.; Bawendi, M. G.; Frangioni, J. V. Renal Clearance of Quantum Dots. *Nat. Biotechnol.* **2007**, *25*, 1165–1170.

32. Takahashi, Y.; Ellis, L. M.; Mai, M. The Angiogenic Switch of Human Colon Cancer Occurs Simultaneous to Initiation of Invasion. *Oncol. Rep.* **2003**, *10*, 9–13.

33. Parikh, R. R.; Yang, Q.; Haffty, B. G. Prognostic Significance of Vascular Endothelial Growth Factor Protein Levels in T1−2 N0 Laryngeal Cancer Treated with Primary Radiation therapy. *Cancer* **2007**, *109*, 566–573.

34. Kedrin, D.; Gligorijevic, B.; Wyckoff, J.; Verkhusha, V. V.; Condeelis, J.; Segall, J. E.; van Rheenen, J. Intravital Imaging of Metastatic Behavior Through a Mammary Imaging Window. *Nat. Methods* **2008**, *5*, 1019–1021.